Optical pattern formation far beyond threshold

T. Ackemann, E. Große Westhoff, M. Pesch, D. Rudolph, and W. Lange

Institut für Angewandte Physik, Westfälische Wilhelms–Universität Münster,

Correnssstr. 2/4, 48149 Münster, Germany

ABSTRACT

Optical pattern formation is studied far beyond threshold in a single-mirror feedback scheme using sodium vapor as the nonlinear medium. Patterns with twelve fundamental wave vectors arise from hexagons in a secondary bifurcation. Besides irregular patterns, quasipatterns and superlattices are obtained. Even after a tertiary bifurcation the patterns remain stationary. Fourier filtering experiments show that the harmonics of the fundamental wave vectors are essential for the stability of the secondary and tertiary patterns. A novel Fourier filtering technique is used for a measurement of the neutral stability curve and proves experimentally the existence of multiple instability regions existing due to the periodicity of the Talbot effect.

Keywords: optical pattern formation, secondary instabilities, quasipatterns, superlattices, Fourier filtering

1. INTRODUCTION

It is a well established fact by now that many of the inhomogeneous spatial states which emerge in the transverse cross section of nonlinear optical systems arise from self-organization phenomena (see e.g.[1,2] for recent reviews). If applications demand a high spatial and temporal coherence of the light field, these phenomena are often annoying. On the other hand, they present beautiful examples for the rather universal phenomenon of spontaneous pattern formation which occurs in many spatially extended nonlinear dissipative systems in nature which are driven far away from thermal equilibrium.[3]

Commonly the uniform state of a pattern forming system is unstable against periodic perturbations with a well defined critical wave number q_c and the resulting patterns are rather simple (stripes, squares, hexagons).[3] More complex behavior might arise from secondary or tertiary bifurcations of these primary patterns. The emergent states are often time dependent and can show an irregular behavior in space and/or time. Probably best studied are the secondary bifurcations from a stripe pattern in Rayleigh-Bénard convection (see[3–5] for reviews). Systems in which the inversion symmetry is broken display hexagonal patterns at threshold.[3,4] A generic secondary bifurcation of these hexagons involves a transition to stripes (e.g. in non-Boussinesq Rayleigh-Bénard convection[6]). The resulting stripe pattern might be ideal and stationary but complex patterns irregular in space and time are also found in the transient or as the asymptotic state (e.g.[7–9]). Related observations were made for a hexagon-square transition.[10] In a special class of optical pattern forming systems (Kerr slice with feedback from a single mirror[11,12]) also a direct transition from a hexagonal to a 'turbulent' state was observed in experiments as well as in numerical simulations.[12–15]

In this paper we report on experimental results on pattern formation far beyond threshold in which the resulting patterns are rather complex but remain regular in space and stationary in time. The resulting patterns have either a high rotational symmetry and are quasiperiodic in space, or a low (six- or fourfold) rotational symmetry but a

E-mail: t.ackemann@uni-muenster.de

complex periodicity. The latter patterns are *superlattices*.[16] Since the experiments indicate that high order instability regions might be of importance, we implement a Fourier filtering technique for a direct measurement of the linear instability properties of the system after the first pattern forming threshold. Optical Fourier filtering techniques open a possibility for investigations of mechanisms of pattern formation which does not exist in non-optical system to our knowledge. However, complex periodic patterns are not confined to optics, they are recently intensively discussed in Faraday experiments in which *two* instabilities are present simultaneously.[17–20] Quasiperiodic and superlattice patterns were also observed in optical systems with broken rotational symmetry.[21]

2. EXPERIMENTAL SETUP AND THE OPTICAL PUMPING NONLINEARITY

The experiment (cf. Fig. 1) is based on the *single feedback mirror arrangement*,[11,12] which is an archetypal system for optical pattern formation (cf. the reviews[1,2,22]). We use sodium vapor in a buffer gas atmosphere as the nonlinear medium (see below).

The light source is a cw ring dye laser which is stabilized in frequency and power. The beam is carefully spatially filtered by transmitting it through a single-mode optical fiber. After the fiber, the beam is collimated (beam waist $w_0 = 1.5\,\mathrm{mm}$), circularly polarized and injected into a vapor cell. The use of an additional telescope consisting of two $f = 100$ mm-lenses allows for a precise adjustment of the position of the beam waist which is placed at the entrance face of the vapor. The cell contains sodium in a nitrogen buffer gas atmosphere (pressure of buffer gas 200-300 hPa). The buffer gas provides strong homogeneous broadening, which masks both the hyperfine splitting and the Doppler broadening of the sodium D_1-line. The length of the heated interaction zone is 15 mm, typical cell temperatures are 310 to 320°C corresponding to a sodium particle density of about 2 to $5 \cdot 10^{13}$ cm^{-3}. A weak longitudinal magnetic field is applied in order to define the axis of quantization.

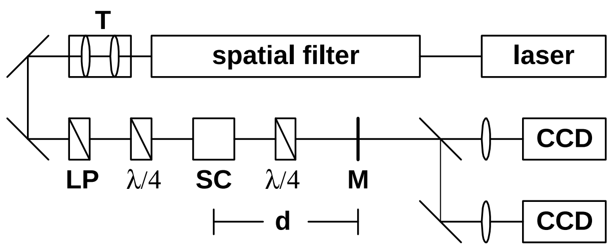

Figure 1. Schematic experimental setup: T: telescope, LP: linear polarizer, $\lambda/4$: quarter-wave plate, SC: sodium cell, M: feedback mirror, CCD: charge coupled camera device.

The transmitted light is fed back into the medium by a plane mirror (reflectivity $R \approx 0.92$) placed at a distance $d = 45...90$ mm behind the medium. A quarter-wave plate is inserted between the cell and the mirror.[23] Its role is discussed below. The intensity distributions of the near field and the far field, which corresponds to the Fourier transform of the former, are monitored with two CCD cameras and are recorded simultaneously.

The experimental conditions are carefully chosen such that the D_1-line can be described as a homogeneously broadened J=1/2→J'=1/2-transition. A formal derivation of the model is given in[24–26]; here we intend only a qualitative discussion. Fig. 2a shows a Kastler diagram of a J=1/2→J'=1/2-transition. Both the excited and the ground state have a two-fold degeneracy. Due to angular momentum selection rules circularly polarized light (let us assume σ_+-light for definiteness) will only induce transitions from the $m_J = -1/2$-state of the ground state to the $m_J = 1/2$-state of the excited state. However, for a sufficiently high buffer gas pressure collisions of sodium with the buffer gas rapidly equalize the population between the Zeeman substates of the excited state, so that the repopulation of the ground state sublevels by relaxation is isotropic. Therefore pumping with circularly polarized light will induce a population difference or *orientation* between the Zeeman sublevels of the ground state.

The complex susceptibility of the vapor depends linearly on the orientation, i.e. there is nonlinear absorption and nonlinear dispersion. The latter one usually dominates since we use detuned excitation.[23,26] The origin of the spatial instability is the fact that any spatial variation of the orientation and hence of the refractive index will cause a phase modulation of the transmitted wave. Diffraction occurring during the propagation in free space from the

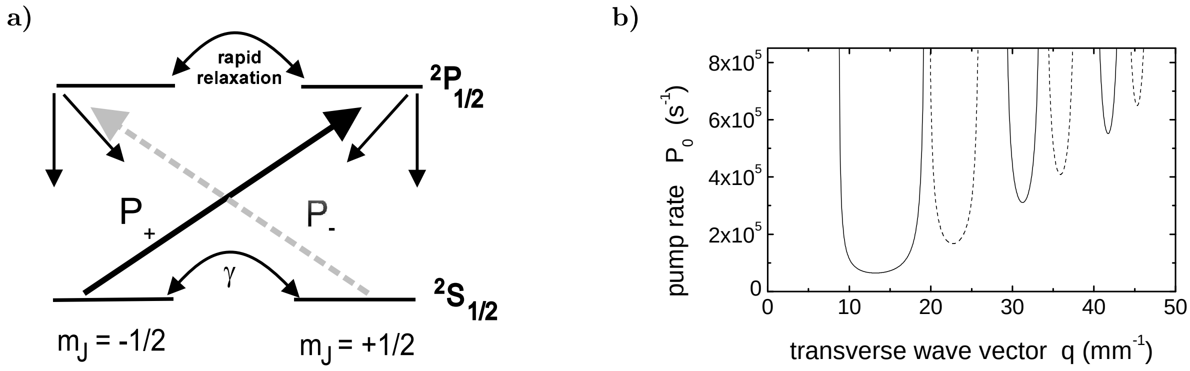

Figure 2. a) Kastler diagram of a J=1/2→J'=1/2-transition driven by σ_+-, respectively σ_+-, light (represented by the solid black, respectively the dashed grey, arrows). b) Typical marginal stability curves for a single-mirror feedback system in a plane spanned by the modulus of the transverse wave vector and the pump rate. The closed lines denote the situation for a negative detuning, the dashed lines for a positive one. The parameters correspond to a typical experimental situation (cf. to Fig. 3, detuning $\Delta = +3.6$ GHz), see[23] for the model equations).

medium to the mirror and back converts the phase modulation to amplitude modulation. This closes a feedback loop since the orientation depends on the intensity of the reentrent light field.

The exchange between amplitude and phase-variation of a periodically modulated plane carrier wave during propagation is known as the Talbot effect.[27,28] The wave number for which this conversion is perfect at a given propagation distance $2d$ will have minimal threshold. For the parameters of Fig. 2b this is the case for $q_c \approx 13$ mm^{-1} for negative detuning and for $q_c \approx 23$ mm^{-1} for positive one. If the power is increased beyond threshold, positive gain is also possible for non-perfect feedback and a whole interval of wave numbers is unstable. This leads to the formation of the tongue-like *instability region* depicted in Fig. 2b. Within this region the homogeneous state is unstable versus a perturbation at the corresponding wave number and a macroscopic spatial pattern can develop.

Furthermore, the Talbot effect is periodic in the direction of propagation, i.e. the original phase modulation is restored exactly at a certain distance. From there, the whole sequence of conversion to amplitude modulation starts again. This implies that – for a given mirror distance d – also considerably higher wave number might experience gain. This leads to the appearance of the additional instability regions depicted in Fig. 2b. For motionless atoms all instability regions would have the same threshold, however the thermal motion of the atoms in a vapor cell leads to a diffusive damping of higher wave numbers.[11,26]

If the vapor is driven by a single circular polarization component, the optical pumping nonlinearity saturates already at rather low input intensities since the relaxation constant γ is small. It turns out that saturation inhibits also pattern formation at high pump power, if there is no additional polarization-changing element in the feedback loop; i.e., it causes the instability regions to close again.[26,29] Hence, pattern formation far beyond threshold cannot be investigated. * The presence of the quarter-wave plate between the cell and the mirror exchanges the polarization state from σ_+ or σ_- in the forward beam to σ_- or σ_+, respectively, in the counterpropagating beam (Fig. 1). Since the two polarization components pump antagonistically (Fig. 2a), a complete saturation of the optical nonlinearity is inhibited. Furthermore, a close inspection shows that the saturation even contributes positively to the pattern formation instability in this specific polarization configuration,[26] thus lowering the threshold. Therefore, the system is very well suited for experimental investigations of pattern formation far above threshold.

3. EXPERIMENTAL RESULTS

The most important control parameters in the experiment are the input power, the detuning from the atomic resonance and the sodium particle density. The latter is a prefactor of the susceptibility and thus parametrizes the

*Actually, it turns out that without the quarter-wave plate the combination of saturation and diffusion even inhibits any instability for the considered parameters[26].

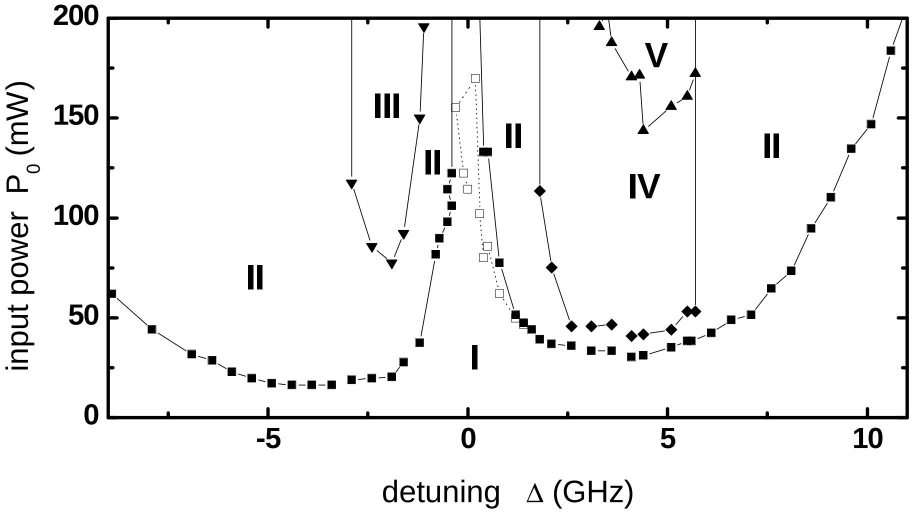

Figure 3. Schematic bifurcation diagram in dependence on the detuning from the sodium-D_1-line and the input power. The boundaries are determined by increasing the power from zero in small steps for fixed detuning. Parameters: nitrogen buffer gas pressure $p_{N_2} = 200\,\mathrm{hPa}$, sodium cell temperature $T = 318\,°\mathrm{C}$, distance between the sodium cell and the feedback mirror $d = 88\,\mathrm{mm}$, reflectivity of the feedback mirror $R = 0.915$. The lines have been added to guide the eyes and to roughly separate the regions of different patterns, which are: I homogeneous state, II hexagons, III stripes (negative detuning), IV patterns with 12 fundamental wave vectors, V squares and stripes. The open squares connected by a dotted line indicate the power at which hexagons give way to the homogeneous state if the power is reduced.

strength of the nonlinearity. We vary it stepwise in the experiment. If the particle density has reached its new equilibrium value, we perform a quasi-continuous scan of power and detuning for fixed cell temperature.

We did not determine the threshold value of the particle density for pattern formation, but for a cell temperature of 280°C patterns are already formed. Since hexagons are the generic patterns at threshold for systems in which the inversion symmetry is broken, hexagons occur. For low particle density, hexagons are the only pattern observed. If the particle density is increased, the complexity of the bifurcation diagram increases: For about 300° a secondary bifurcation of hexagons to stripes occurs, if the laser power is increased beyond the first threshold. The bifurcation diagram for 318°C is depicted in Fig. 3. The parameter space can roughly be divided into five regions.

For increasing input power the homogeneous state (region I) bifurcates to hexagonal patterns (region II). This bifurcation takes place for both signs of detuning. The minimal threshold is about 17 mW for negative detuning and 30 mW for positive detuning. The asymmetry in the first threshold between the two sides of the resonance is explained by the fact that the wave number and therefore the damping by diffusion is higher (cf. to Fig. 2b, also[23]).

If the power is increased from zero for zero detuning, one does not encounter patterns up to the highest power level experimentally accessible. However, patterns persist even at resonance, if the detuning is reduced to zero at fixed power after the threshold for pattern formation was crossed for a high value of the detuning. The values of power were they vanish, if the power is reduced again, is denoted in Fig. 3 by the open squares connected by the dotted line. This demonstrates that there is a rather extended region with bistability between the homogeneous state and hexagons in the vicinity of the resonance, i.e. the bifurcation is clearly subcritical.

The rather low value of the threshold enables one to perform investigations up to twelve, respectively six (depending on the sign of detuning), times the threshold power. For negative detuning only a secondary bifurcation to stripes occurs (region III).

For positive detuning the behavior is more complex. In the region of parameter space denoted by IV in Fig. 3 patterns consisting of twelve wave vectors with the same or nearly the same wave number emerge in a secondary bifurcation of hexagons. Depending on the exact configuration of wave vectors the resulting patterns might be irregular, quasiperiodic or complex periodic (superlattices). At the maximum input power (in region V) there is

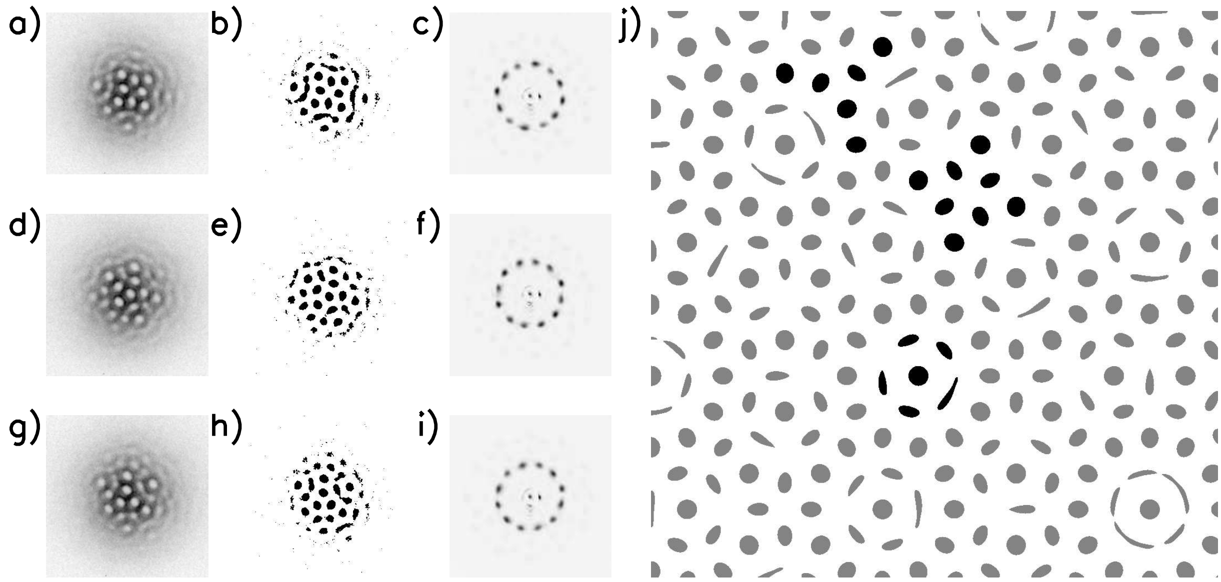

Figure 4. Experimentally observed near field intensity distributions (a, d, g), contrast enhanced near field image after binary thresholding (b, e, h) and far field intensity distribution of quasipatterns (c, f, i) for constant parameters. The image on the right (j) shows a numerically generated ideal quasipattern after binary thresholding. Parameters: $p_{\mathrm{N}_2} = 200\,\mathrm{hPa}$, $T = 281\,^{\circ}\mathrm{C}$ (but $L = 40$ mm), $\Delta = +4.1$ GHz, $d = 97\,\mathrm{mm}$, $P_0 = 47$ mW.

another transition to patterns which are 'simple periodic' again. We observe square and stripe patterns. Their modulation depth is very high and the transition between bright and dark regions very abrupt. Correspondingly, the far field images show a strong excitation of harmonics. It can be noted that − though the system has undergone already a quite complicated sequence of bifurcations − the patterns are still stationary and this last (within the experimentally accessible range of power) bifurcation lowers the apparent spatial complexity again.

As already mentioned the common characteristic of the patterns in region IV is that they consist of twelve fundamental wave vectors of nearly the same wave number. Which of these patterns dominates in specific parts of region IV depends on other parameters, e.g. the mirror distance. Furthermore, there is the possibility of multistability. A detailed characterization has to be left to a future paper.

In a typical scenario a first transition occurs from hexagons to patterns in which the wave numbers of the twelve wave vectors and the angle between neighboring wave vectors are the same within the experimental resolution.[30] This implies a 12fold rotational symmetry. The far field images are displayed in the third column of Fig. 4. From theoretical considerations it is known that a rotational symmetry higher than six is incompatible with translational symmetry, the corresponding pattern in real space is a quasiperiodic pattern (e.g.[31]). An example is depicted in Fig. 4j which was obtained by superimposing numerically six cosine waves of the same amplitude and phase at a mutual angle of 30°. Binary thresholding was applied to emphasize the main features. Locally, there is a rather high degree of order and one can identify certain features which appear again and again in the pattern (some prominent ones are highlighted in the image). However, there is no long-range order or periodicity.

In the experiment we observe different near field patterns for constant parameters (and the same far field image) which appear to be rather irregular (first column of Fig. 4). However, comparing contrast enhanced versions of these patterns (second column of Fig. 4) with the ideal quasipattern in Fig. 4j, one realizes that the experimentally observed images are parts of a spatially extended quasipattern: The four-fold structure in Fig. 4b appears, for example, close to the upper right of the center, the pentagon surrounded by a twelve-fold ring (Fig. 4e) just below the center, and the three-fold cross (Fig. 4h) in the upper left part of Fig. 4j. The corresponding structures are emphasized to guide the eye in Fig. 4j.

In the more general case, the wave number and the angles between the wave vectors are not necessarily equal but show small deviations from each other. A rather complicated situation is depicted in Fig. 5 which corresponds

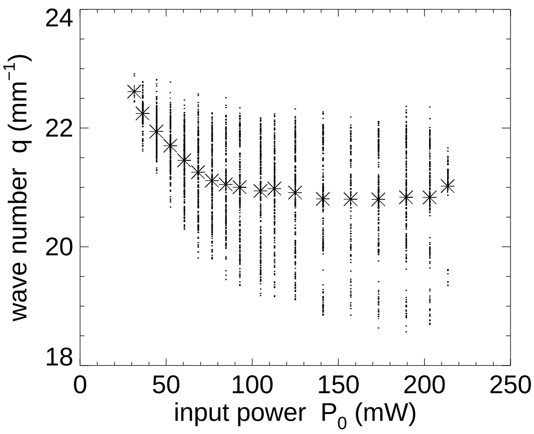

Figure 5. Wave number of modes in Fourier space in dependence on input power. For each input power about 20 images were analyzed. Single dots denote the wave number of one single mode, the crosses are obtained by averaging over all wave numbers. Note that the large spread is due to the fact that several patterns with different wave numbers coexist typically for the same power for these parameters. Parameters as in Fig. 3, $\Delta = 3.6$ GHz.

approximately to the detuning with the minimal threshold in Fig. 3. The figure shows a kind of diagram in the space spanned by the transverse wave number and power, in which each of the small dots represents the modulus of a single fundamental wave vector of about 20 images which were acquired and analyzed for each power level. It is obvious that the spread in wave number increases with increasing power. The maximum ratio between the lowest and the highest wave number observed occurs at 190 mW and amounts to about 1.2. This spread in wave number probably reflects the fact that intervals of wave numbers with increasing width become linearly unstable after the first threshold is crossed (cf. Fig. 2b), i.e. there are more degrees of freedom available for pattern formation. At the same time the average wave number decreases. The interpretation of this observation is unclear in the present stage of investigation.

The observation that the distribution of the observed wave numbers in Fig. 5 appears to be more or less dense indicates that different kinds of patterns with different configurations of wave vectors coexist at the same power level. Indeed, in many patterns there is no apparent regularity in the deviations from the 12-fold arrangements. These do not have a regularity in real space, either, and we are not aware of any tools to provide a further characterization. However, the twelve wave vectors can also rearrange such that they lie again on a lattice in Fourier space. The modulus of the wave vectors spanning this lattice – i.e. the wave vectors of the reciprocal grid – is much smaller than the wave number of the fundamental wave vectors. This is the fingerprint of a superlattice. We observe two kinds of superlattices. One of them is based on a four-fold symmetry in Fourier space, the other on a six-fold symmetry. A detailed characterization and discussion of these superlattices will be provided in a forthcoming paper.

4. FOURIER FILTERING

4.1. Modification of Experimental Setup

A close inspection of the far field images in Fig. 4 reveals that harmonics of the fundamental wave vectors are excited. In order to investigate the relevance of these harmonics in the stabilization of the complex patterns, we set up a Fourier filtering experiment. Wave number-selective feedback was suggested[32] and experimentally demonstrated[15,33–36] to be a very powerful tool for stabilizing and tracking unstable states. Furthermore it was demonstrated that it can be used to investigate and validate scenarios of pattern formation which are difficult to access otherwise.[34,35]

A telescope in a $4f$-setup consisting of AR-coated, plano-convex, $f = 100$ mm-lenses is inserted in the feedback loop (Fig. 6). An iris is placed in the focal plane between the lenses at which the Fourier transform of the optical field is accessible.

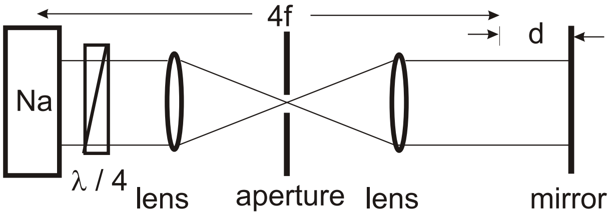

Figure 6. Modified setup with a 1:1 telescope focused to infinity inserted in the feedback loop.

4.2. Experimental Results: Fourier Filtering of Complex Patterns

The filtering operation is illustrated for twelvefold quasipatterns in Fig. 7. If the aperture is open, the pattern is not affected (Fig. 7a,g). It survives also if an aperture with a sufficiently large radius is introduced (Fig. 7b,h), but gives way to a hexagonal pattern if the cut-off frequency is decreased to about two times the fundamental wave vector. The subfigures i and j of Fig. 7 were taken at the same radius of the aperture, one shows quasipatterns, the other hexagons. There is a slight increase in wave number (about 1%) if the hexagon forms. Obviously, the harmonics formed by addition of two neighboring wave vectors on the intersection of the angle start to 'feel' the iris due to their finite width (They are positioned at $q_3 = 2\cos(\pi/12)q_0 \approx 1.93q_0$.). If the radius of the aperture is reduced further, hexagons are still stable (Fig. 7e,k and Fig. 7f,l). This observation demonstrates clearly that harmonics are not necessary for the stabilization of hexagons.

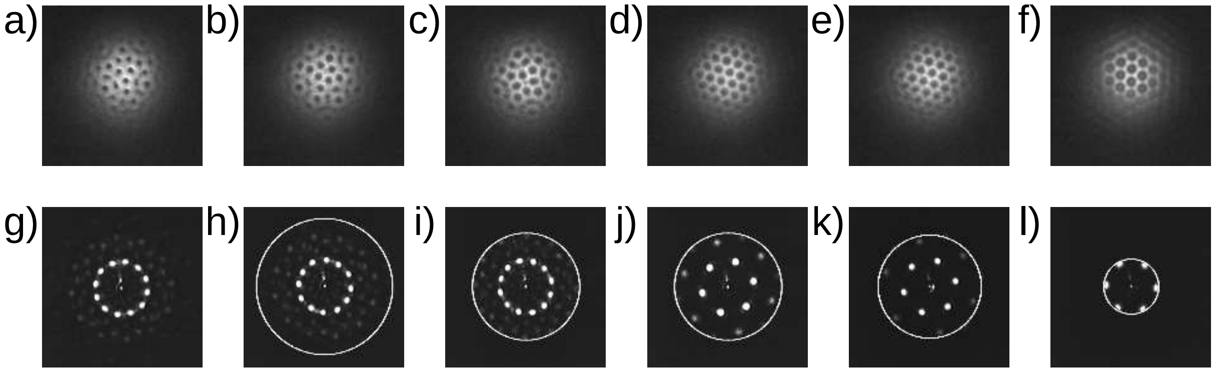

Figure 7. Sequence of images demonstrating the destabilization of quasipatterns if the cut-off frequency of a low-pass filter in Fourier space is reduced. Upper row: near field intensity distributions (size 4.44 mm × 4.44 mm); lower row: far field intensity distributions ($q_{\text{max}} = 76.9\ \text{mm}^{-1}$). Parameters: $p_{N_2} = 200\,\text{hPa}$, $T = 318\,°\text{C}$, $\Delta = +5$ GHz, $d = 87\,\text{mm}$, $P_0 = 70$ mW. The cut-off wave number is indicated in the far field images by the white circle. Its ratio compared to the wave number of the unperturbed wave number q_0 (in image g) is in g) ∞, h) 2.57, i) 2.02, j) 2.02, k) 1.94, l) 1.02.

In a very similar way, the superlattices give way to hexagons if the iris is closed far enough to suppress the Fourier components at approximately $2q_0$. This indicates a stabilization mechanism of the complex periodic patterns via higher harmonics. Also for the patterns in region V in Fig. 3, a suppression of the higher harmonics in a Fourier filtering experiment results in the formation of hexagonal patterns.

4.3. Measurement of Instability Regions

Since the analysis of Fig. 5 indicates that the width of the fundamental instability region might be of importance for the process of pattern selection, the question arises whether the width of the first instability region can be determined experimentally. Furthermore, the positions of the minima of the dashed instability regions depicted in Fig. 2 suggest that the importance of the harmonics of the fundamental modes revealed in the filtering experiment in Fig. 7 might be due to a near-resonance of the harmonics with the third instability region. This motivates the search for an experimental method to determine also threshold, shape and width of the high order instability regions. In general, this is difficult since Fig. 10b represents the growth rate of an inhomogeneous perturbation from the homogeneous state. After the first threshold, however, a pattern already developed and one cannot isolate a growth rate from a homogeneous state anymore. Obviously, one has to confine the dynamics to wave vectors with a single wave number. Furthermore it appears to be beneficial to suppress the possibility of bistability or other cooperative dynamics by selecting a single wave vector (and its complex conjugate). This means that one has to develop a filter to select a single stripe pattern with arbitrary wave number. [†]

Fig. 8 illustrates the steps in the filter design. The upper row displays the schematics of the filter, the middle row the resulting pattern in near field and the lower row the corresponding wave vectors in Fourier space. The left column shows the situation without filtering, for which hexagons are stable for the parameters chosen. By introducing a slit stripes can be stabilized (second column to the left in Fig. 8). This result is well known.[15,34,35] Since the far field spots can be considered to arise from the diffraction of the input field at a stationary refractive index grating in the medium,[22] any wave vector appearing in the observed patterns is accompanied by its complex conjugate. Therefore it is sufficient to do the filtering with a half-plane and still a stripe pattern is selected (second column to the right in Fig. 8). However, its wave vector still corresponds to the minimum q_c of the instability region. The magnitude of the wave vector can be controlled, if an additional band pass filter is introduced. By this means, one can obtain stripe patterns of arbitrary wave number (as long as the underlying wave number becomes linear unstable for some power level). This result is demonstrated in the rightmost column of Fig. 8. The wave number of the evolving Fourier modes is considerably higher and the period of the stripes in real space shorter than without the band pass.

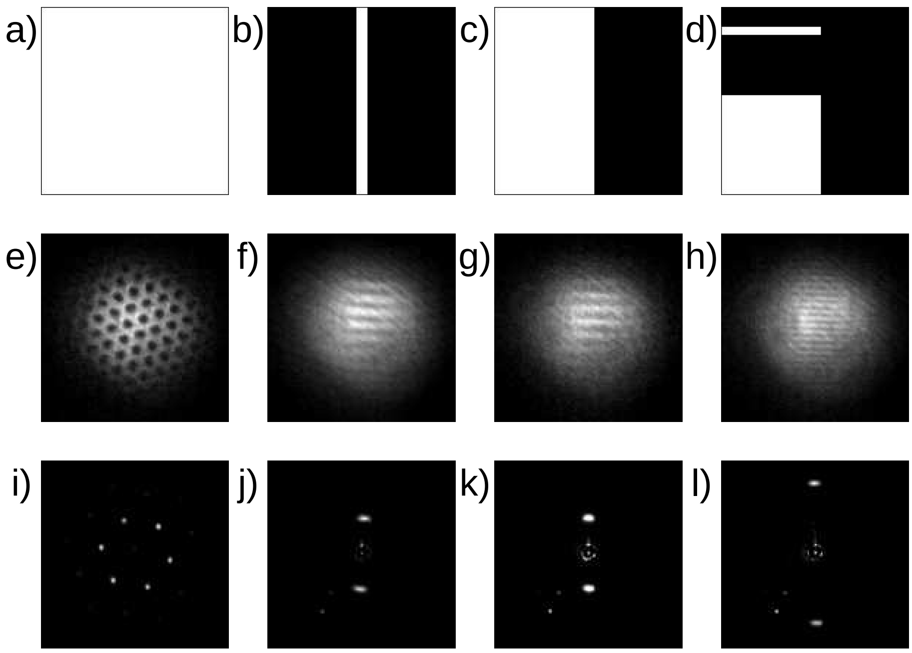

Figure 8. Sequence of images demonstrating the method used to select stripe patterns with a chosen wave number. Upper row: filtering aperture, black denotes opaque parts, white transparent; middle row: near field intensity distributions; lower row: far field intensity distributions. Parameters: $p_{\mathrm{N}_2} = 309$ hPa, $T = 311.4°$ C, $\Delta = +8$ GHz, $d = 77$ mm, e) $P_0 = 160$ mW, f) $P_0 = 50$ mW, g) $P_0 = 45$ mW, h) $P_0 = 187$ mW.

In the experiment, the half-plane was implemented by a blade and the band-pass by wires. Different diameters of wires have to be used in order to be able to change the wave number over all the interesting area up to about

[†]If the goal of the experiment is not only to check for the instability of the homogeneous state but also to determine the true stripe solution, one has to allow also for the harmonics to pass.

55 mm^{-1}. For higher wave numbers the available laser power is not sufficient to induce an instability. The lowest instability region is depicted in Fig. 9. It has the typical nearly parabolic shape expected from the linear stability analysis and its minimal threshold agrees to the one of the hexagons in the system without a filter.

Within the accessible range we obtain three instability regions. Their thresholds increase with increasing wave number. All these features are in very good qualitative agreement with the prediction of Fig. 2b. However, a close comparison reveals quantitative differences. The results show that in tendency the damping is higher in the experiment than predicted by the linear stability analysis. Numerical simulations show that this discrepancy can be traced back to the fact that in the experiment a Gaussian beam is used whereas the linear stability analysis assumes an infinite homogeneous state. Detailed experimental and theoretical results will be presented in a forth-coming paper, if a semi-analytical analysis of finite-size effects is accomplished.

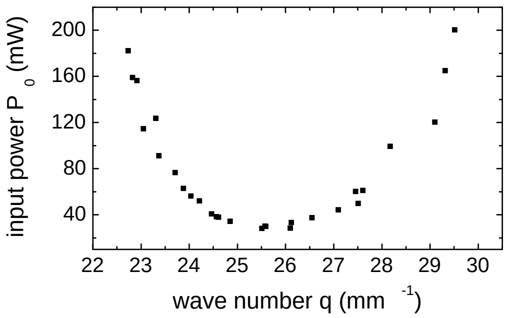

Figure 9. Threshold in dependence on wave number for the first instability region. Parameters: $p_{\mathrm{N}_2} = 306$ hPa, $T = 316°$ C, $\Delta = +5.4$ GHz, $d = 77$ mm, $R = 0.99$.

The experiments show that the third instability region is still damped if the secondary bifurcation to the patterns with twelve wave vector occurs. The threshold of the third region, however, corresponds nicely to the threshold for the formation of the stripes and squares (region V), i.e. they seem to form if the third region becomes active. We did not see a correspondence between the threshold for the second region and any bifurcation in the unfiltered system. This might be due to the fact that the second region does not participate in resonant interactions.

5. INTERPRETATION

In this Subsection, we want to convey the idea, why the stability of these structures might depend on the presence of their harmonics. Pattern selection beyond threshold is usually described by amplitude equations for the complex amplitudes A_i of the involved Fourier modes with wave vectors $\mathbf{q_i}$ ($|\mathbf{q_i}| = q_0$ [‡]). If the nonlinearities provide saturation already at cubic order, the amplitude equation for the mode 1 is given by[4,31,37]

$$\frac{\partial A_1}{\partial t} = \mu A_1 + \sum_{i,j} \eta A_i^\star A_j^\star \delta(\mathbf{q_1} + \mathbf{q_i} + \mathbf{q_j}) - \gamma A_1 |A_1|^2 + A_1 \sum_{i=2}^{N} \zeta(\alpha_i) |A_i|^2. \tag{1}$$

The equations for the other modes are obtained by proper permutations of the indices. The linear term describes the linear growth of a single mode from the homogeneous state. The quadratic terms result in a resonant wave vector interaction (*hexagonal triad*) that is responsible for the formation of hexagons.[4] The two last terms describe self- and cross-saturation in cubic order. The cross-saturating term depends on the angle α_i between the wave vector of the mode i and the one of mode 1. Fig. 10a illustrates the wave vector coupling leading to the cross-saturation of the mode $\mathbf{q_1}$ by the mode $\mathbf{q_2}$. It involves the harmonics $\mathbf{Q_2} = \mathbf{q_1} + \mathbf{q_2}$ or $\mathbf{Q_1} = \mathbf{q_1} - \mathbf{q_2}$ as intermediate states. The measurement of the threshold of the high order instability regions discussed in the previous Subsection showed that the harmonics of the quasipatterns are still passive, i.e. their growth rate is smaller than zero. Thus their amplitude dynamics can be adiabatically eliminated. This justifies also the restriction to equations of motion for

[‡]Due to this limitation to equal wave numbers we have to confine to the discussion of quasipatterns for the moment. For the superlattices with different wave numbers the usual theory needs to be extended. However, the physical mechanism is expected to remain the same.

the fundamental modes assumed in Eq. (1). Under these conditions it turns out that the linear growth coefficient for each of these harmonics enters the expression for the cross-coupling coefficient in the denominator (e.g.[38]). This means that the cross-coupling coefficient depends on the angle α between the two modes since the modulus of the harmonics and thus the growth rate depends on α. If the wave number of the harmonics is only weakly damped, the coupling can be resonantly enhanced. This is reminiscent of the relevance of virtual levels for multi-photon processes in conventional nonlinear optics. Fig. 10b shows that this situation is encountered in the system under investigation if the angle between the wave vectors is 30°, i.e. for a 12fold quasipattern. In that case the harmonics are nearly resonant with the third instability region. Due to the resonance-like dependence this might have considerable consequences even if the harmonics are still passive.

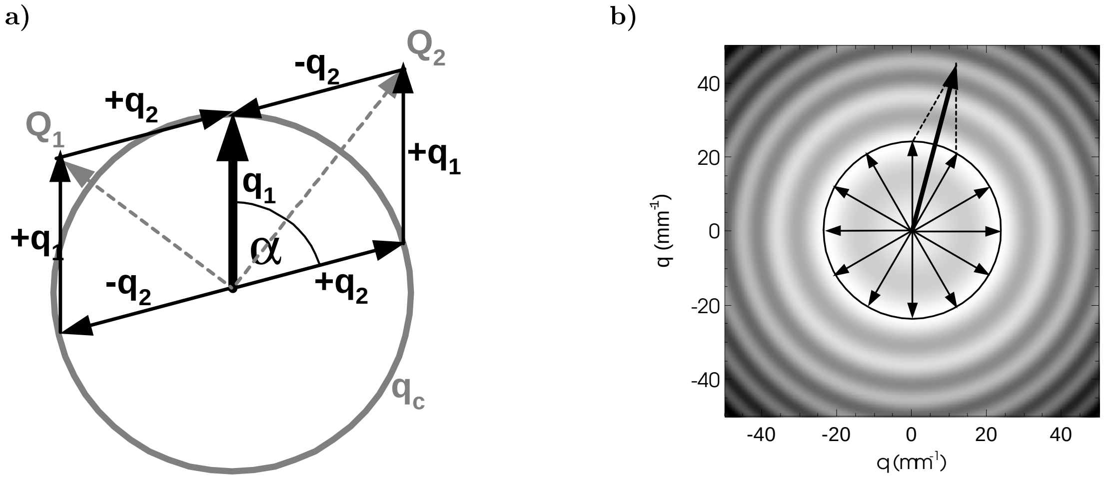

Figure 10. a) Wave vector diagram illustrating the wave vector coupling leading to cross-saturation of the mode $\mathbf{q_1}$ by the mode $\mathbf{q_2}$. b) Growth rate for Fourier modes with a wave vector (q_x, q_y) determined from a linear stability analysis of the homogeneous state at threshold. The coding is in a linear grey level scale with white denoting zero (i.e. maximum) growth rate. The wave vector diagram illustrates that the harmonics of two fundamental wave vectors of a 12fold quasipattern are resonant with a local maximum of the linear growth rate. Parameters: $p_{\mathrm{N}_2} = 200\,\mathrm{hPa}$, $T = 317\,°\mathrm{C}$, $\Delta = +3.6\,\mathrm{GHz}$, $d = 88\,\mathrm{mm}$, $P_0 = 51$ mW.

This qualitative reasoning has to be put on firm mathematical ground, of course, by calculating the coefficients of the amplitude equations by a nonlinear stability analysis. For the system without the quarter wave-plate (and a simplified description of the atomic diffusion) Le Berre et al. predicted the appearance of 12fold quasipatterns at threshold for low diffusion rates and negative detuning.[37] Since the quarter-wave plate compensates – at least in the limit of no absorption and no diffusion – the exchange of wave numbers taking place if the sign of detuning changes,[23,26,39] the instability regions considered by Le Berre el al. are essentially the ones which are also relevant in our experiment. Therefore a modification of their calculations might explain the secondary bifurcation from hexagons to quasipatterns in our system, too. The fact that passive high order instability regions existing in optical systems are beneficial for obtaining quasipatterns was noticed before.[37,40,41] Also the stabilization of superlattices (with only one wave vector) was related to passive higher harmonics in a recent paper.[38]

6. INFLUENCE OF WAVEFRONT CURVATURE

In the beginning of the experiments the beam parameters of the input beam were determined only by the outcoupling lens of the optical fiber used as spatial filter. In this setup it was sometimes difficult to reproduce details of the bifurcation diagram, e.g. the formation of squares. The insertion of the additional telescope (cf. Section 2) gave the necessary degrees of freedom for a fine adjustment of the position of the beam waist. It turns out that one has to control the position of the waist on the level of about 30 cm in order to achieve reproducible results. [§]

We performed preliminary experiments in which the input beam was adjusted to be slightly convergent or divergent on purpose. We observe quantitative corrections compared to the situation of best collimation, e.g. the width

[§]This positioning accuracy has to be compared with the Rayleigh length of the beam which is about 11 m.

in detuning space of the region IV with secondary patterns changes. Qualitatively new features also exist, e.g. a new superlattice on a rhombic grid appears for a slightly diverging beam. This indicates that the wavefront curvature of the input beam is an important parameter one has to control in experiments.

7. CONCLUSION

In conclusion, we observed the formation of stationary patterns in a secondary bifurcation from hexagons and even in a tertiary bifurcation. In the secondary bifurcation typically patterns built from 12 wave vectors of equal or slightly unequal length occur. Fourier filtering experiments established that the harmonics are important for their stabilization. The existence of multiple instability regions was also directly demonstrated by using a band-pass filter in Fourier space.

Furthermore, a detailed analysis of the experiments indicates that finite-size and wavefront curvature effects have even to be taken into account if the structures display rather well defined peaks in Fourier space. Corresponding investigations are under way.

ACKNOWLEDGMENTS

We gratefully acknowledge financial support by the Deutsche Forschungsgemeinschaft and the collaboration with R. Herrero in the early stages of the investigations.

REFERENCES

1. F. T. Arecchi, S. Boccaletti, and P. L. Ramazza, "Pattern formation and competition in nonlinear optics," *Phys. Rep.* **318**, pp. 1–83, 1999.
2. L. A. Lugiato, M. Brambilla, and A. Gatti, "Optical pattern formation," *Adv. Atom. Mol. Opt. Phys.* **40**, pp. 229–306, 1999.
3. M. C. Cross and P. C. Hohenberg, "Pattern formation outside of equilibrium," *Rev. Mod. Phys.* **65**, pp. 851–1112, 1993.
4. F. H. Busse, "Non-linear properties of thermal convection," *Rep. Prog. Phys.* **41**, pp. 1929–1967, 1978.
5. F. H. Busse and R. M. Clever, "Mechanisms of the onset of time-dependence in thermal convection," in *Time-dependent nonlinear convection*, P. A. Tyrand, ed., pp. 1–49, Computational Mechanics Publications, Boston, 1998.
6. S. Ciliberto, E. Pampaloni, and C. Pérez-García, "Competition between different symmetries in convective patterns," *Phys. Rev. Lett.* **61**, pp. 1198–1201, 1988.
7. Q. Ouyang and H. L. Swinney, "Transition to chemical turbulence," *Chaos* **1**, pp. 411–420, 1991.
8. W. Lange, Y. A. Logvin, and T. Ackemann, "Spontaneous optical patterns in an atomic vapor: observation and simulation," *Physica D* **96**, pp. 230–241, 1996.
9. Y. Astrov, E. Ammelt, and H.-G. Purwins, "Experimental evidence for zigzag instability of solitary stripes in a gas discharge system," *Phys. Rev. Lett.* **78**, pp. 3129–3132, 1997.
10. A. Aumann, T. Ackemann, E. G. Westhoff, and W. Lange, "Transition to spatio-temporally irregular states in a single-mirror feedback system," *Int. J. Bif. Chaos* , 2001. Accepted for publication.
11. W. J. Firth, "Spatial instabilities in a Kerr medium with single feedback mirror," *J. Mod. Opt.* **37**, pp. 151–153, 1990.
12. G. D'Alessandro and W. J. Firth, "Hexagonal spatial pattern for a Kerr slice with a feedback mirror," *Phys. Rev. A* **46**, pp. 537–548, 1992.
13. R. Neubecker, B. Thuering, and T. Tschudi, "Formation and characterization of hexagonal patterns in a single feedback experiment," *Chaos, Solitons & Fractals* **4**, pp. 1307–1322, 1994.
14. F. Castaldo, D. Paparo, and E. Santamato, "Chaotic and hexagonal spontaneous pattern formation in the cross-section of a laser beam in a defocusing Kerr-like film with single feedback mirror," *Opt. Commun.* **143**, pp. 157–161, 1997.
15. A. V. Mamaev and M. Saffman, "Selection of unstable patterns and control of optical turbulence by Fourier plane filtering," *Phys. Rev. Lett.* **80**, pp. 3499–3503, 1998.
16. U. Dahmen *Encyclopedia of physical science and technology* **10**, p. 319, 1987.

17. A. Kudrolli, B. Pier, and J. P. Gollub, "Superlattice patterns in surface waves," *Physica D* **123**, pp. 99–111, 1998.
18. H. Arbell and J. Fineberg, "Spatial and temporal dynamics of two interacting modes in parametrically driven surface waves," *Phys. Rev. Lett.* **81**, pp. 4384–4387, 1998.
19. C. Wagner, H. W. Müller, and K. Knorr, "Crossover from a square to a hexagonal pattern in Faraday surface waves," *Phys. Rev. E* **62**, pp. R33–R36, 2000.
20. H.-J. Pi, S. Park, J. Lee, and K. Lee, "Superlattice, rhombus, square, and hexagonal standing waves in magnetically driven ferrofluid surface," *Phys. Rev. Lett.* **84**, pp. 5316–5319, 2000.
21. E. Pampaloni, S. Soria, and F. T. Arecchi, "Phase locking in nonlinear optical patterns," *Phys. Rev. Lett.* **78**, pp. 1042–1045, 1997.
22. T. Ackemann and W. Lange, "Optical pattern formation in alkali metal vapors: Mechanisms, phenomena and use," *Appl. Phys. B* **72**, pp. 21–34, 2001.
23. A. Aumann, E. G. Westhoff, R. Herrero, T. Ackemann, and W. Lange, "Interplay of dispersion and absorption in a new optical pattern-forming system," *J. Opt. B: Quantum Semiclass. Opt.* **1**, pp. 166–170, 1999.
24. F. Mitschke, R. Deserno, W. Lange, and J. Mlynek, "Magnetically induced optical self-pulsing in a nonlinear resonator," *Phys. Rev. A* **33**, pp. 3219–3231, 1986.
25. M. Möller and W. Lange, "Radiation trapping: a new mechanism for chaos in a nonlinear optical resonator," *Phys. Rev. A* **49**, pp. 4161–4169, 1994.
26. T. Ackemann, A. Aumann, E. G. Westhoff, Y. A. Logvin, and W. Lange, "Polarization degrees of freedom in optical pattern forming systems: alkali metal vapor in a single-mirror arrangement," *J. Opt. B: Quantum Semiclass. Opt.* **3**, pp. S124–S132, 2001.
27. W. H. F. Talbot, "Facts relating to optical science. No. IV," *Philos. Mag.* **9**(Third series), pp. 401–407, 1836.
28. E. Ciaramella, M. Tamburrini, and E. Santamato, "Talbot assisted hexagonal beam patterning in a thin liquid crystal film with a single feedback mirror at negative distance," *Appl. Phys. Lett.* **63**, pp. 1604–1606, 1993.
29. R. Neubecker, G. L. Oppo, B. Thuering, and T. Tschudi, "Pattern formation in a liquid crystal light valve with feedback, including polarization, saturation, and internal threshold effects," *Phys. Rev. A* **52**, pp. 791–808, 1995.
30. R. Herrero, E. G. Westhoff, A. Aumann, T. Ackemann, Y. A. Logvin, and W. Lange, "Twelvefold quasiperiodic patterns in a nonlinear optical system with continuous rotational symmetry," *Phys. Rev. Lett.* **82**, pp. 4627–4630, 1999.
31. B. A. Malomed, A. A. Nepomnyashchii, and M. I. Tribel'skii, "Two-dimensional quasiperiodic structures in non equilibrium systems," *Sov. Phys. JETP* **69**, pp. 388–396, 1989.
32. R. Martin, A. J. Scroggie, G.-L. Oppo, and W. J. Firth, "Stabilization, selection and tracking of unstable patterns by Fourier space techniques," *Phys. Rev. Lett.* **77**, pp. 4007–4010, 1996.
33. S. J. Jensen, M. Schwab, and C. Denz, "Manipulation, stabilization, and control of pattern formation using fourier space filtering," *Phys. Rev. Lett.* **81**, pp. 1614–1617, 1998.
34. T. Ackemann, B. Giese, B. Schäpers, and W. Lange, "Investigation of pattern forming mechanisms by Fourier filtering: properties of hexagons and the transition to stripes in an anisotropic system," *J. Opt. B: Quantum Semiclass. Opt.* **1**, pp. 70–76, 1999.
35. T. Ackemann, B. Schäpers, J. P. Seipenbusch, Y. A. Logvin, and W. Lange, "Drifting and locking behavior of optical patterns - an analysis using Fourier filtering," *Chaos, Solitons & Fractals* **10**, pp. 665–673, 1999.
36. E. Benkler, M. Kreuzer, R. Neubecker, and T. Tschudi, "Experimental control of unstable patterns and elimination of spatiotemporal disorder in nonlinear optics," *Phys. Rev. Lett.* **84**, pp. 879–882, 2000.
37. M. L. Berre, D. Leduc, E. Ressayre, and A. Tallet, "Optical quasipatterns and multicriticality," *Asian J. Phys.* **7**, pp. 483–494, 1998.
38. M. Silber, C. M. Topaz, and A. C. Skeldon, "Two-frequency forced Faraday waves: weakly damped modes and pattern selection," *Physica D* **143**, pp. 205–225, 2000.
39. A. J. Scroggie and W. J. Firth, "Pattern formation in an alkali-metal vapor with a feedback mirror," *Phys. Rev. A* **53**, pp. 2752–2764, 1996.
40. E. V. Degtiarev and M. A. Vorontsov, "Dodecagonal patterns in a Kerr-slice/feedback-mirror type optical system," *J. Mod. Opt.* **43**, pp. 93–98, 1996.
41. L. M. Pismen and B. Y. Rubenstein, "Quasiperiodic and dynamic planforms in nonlinear optics," *Chaos, Solitons & Fractals* **10**, pp. 761–776, 1999.